2009

Development of Novel Semisolid Powder Processing for Micromanufacturing

Yufeng Wu
Iowa State University

Development of novel semisolid powder processing for micromanufacturing

by

Yufeng Wu

A thesis submitted to the graduate faculty

in partial fulfillment of the requirements for the degree of

MASTER OF SCIENCE

Major: Mechanical Engineering

Program of Study Committee:
Gap-Yong Kim, Major Advisor
Iver Anderson
Shankar Subramaniam

Iowa State University

Ames, Iowa

2009

TABLE OF CONTENT

LIST OF FIGURES

LIST OF TABLES

ACKNOWLEDGEMENTS

I would like to take this opportunity to express my thanks to those who helped me with various aspects of conducting research and the writing of this thesis. First and foremost, thank Dr. Gap-Yong Kim for his guidance, patience and support throughout this research and the writing of this thesis. I would also like to thank my committee members, Dr. Shankar Subramaniam and Dr. Iver Anderson, for their efforts and contribution to this work. Finally, I would thank my parents, Zhengzhong Wu and Baolian Cheng, and my girlfriend Jing Ren for their invaluable supports and help in my study in the United State.

ABSTRACT

Semisolid powder processing (SPP) is a promising approach for near net-shape forming of features in micro/meso-scale. By combining the concept of forming in the semisolid state and conventional powder metallurgy, SPP provides a novel solution to various processing and materials engineering challenges faced in micromanufacturing. Replacing bulk materials with powdered materials adds a new dimension to the traditional semisolid technique by allowing tailoring of material properties. In this dissertation, experimental study to understand flow characteristics of metallic powders in the semisolid state is performed, and its potential application to the fabrication of a functionally graded structure (FGS) is demonstrated.

The viscosity and phase segregation behavior of Al-Si powders in the semisolid state were first studied with back extrusion experiments. Effects of process parameters including shear rate, extrusion ratio, heating time and pre-compaction pressure were analyzed using the design of experiments method. The results showed that the effects of shear rate, extrusion ratio and heating time were statistically significant factors influencing the viscosity. The semisolid state powders showed a shear thinning behavior. Moreover, microstructure analysis of extruded parts indicated severe phase segregation during the forming process. As the extrusion opening became small (~400 μm), the phase segregation increased.

A two-layer FGS with one layer reinforced by SiC particles was fabricated with SPP. The results indicate that SPP is capable of fabricating graded structures with promising microstructures and mechanical properties. When the SiC particles are larger than the matrix

powder, dense and strong parts were formed. Smaller SiC particles can isolate the metal powders and result in porous and weak structures. The roughness of the SiC particle surface affects interface bonding between SiC particles and Al-Si-Cu matrix phase.

In summary, SPP has the potential to become a viable micromanufacturing method that can be used to make graded structures with low cost, good microstructure and promising properties.

CHAPTER 1. INTRODUCTION

1.1 Motivation

There has been increasing demand for 3-D micro-parts for applications in integrated electronic devices, sensors, micro-actuation systems and energy devices [1]. Current micro-manufacturing methods, however, are not able to satisfy the needs arising from various industrial sectors, especially when mass production is considered. Recently, techniques involving processing of metallic alloys in the semisolid state [2-7] have been studied due to their advantages over conventional forging [8] and casting [9] processes. The unique behavior of the material having both the liquid and solid phases enables the forming of complex shapes at reduced loads. The potential of applying the technology to micro/meso-scale part fabrication has also been reported [2-4].

This study further expands the semisolid processing technology by exploring the use of powdered materials for manufacturing of micro-parts instead of using typical bulk materials. Semisolid bulk forming requires break-down of the dendritic microstructure in the feedstock alloy materials. Replacing the bulk materials with powders enables mixing of various powders for improved properties and eliminates post-processing steps required for powder metallurgy routes. As a result, this allows discovery of new fabrication route for micro-parts, adds a new dimension to traditional semisolid processing by allowing tailoring of the material properties, and may lead to new ways to make functionally graded structures in composite materials.

Therefore, the motivation of this research is to assess the potentials of the new fabrication technique that utilizes the metallic powders in the semisolid state and to lay a fundamental foundation that will allow a scientific approach needed to characterize the novel process. First, the knowledge gap in understanding the flow of powders in the semisolid state needs to be filled. Second, understanding of phase segregation at the micro-length scales is needed as this becomes evident when the feature size becomes small. Third, the composite formation mechanism between the reinforcement particles and semisolid powder matrix must be understood. Fourth, gradient structure formation and transportation of reinforcement particles needs to be understood.

1.2 Research Framework and Objectives

This study aimed to: 1) understand the phase segregation phenomenon and rheology characteristics in SPP for micro/meso scale part fabrication; 2) understand the formation mechanism of composites (especially FGS composites) by SPP.

Materials in the semisolid state can experience phase segregation during the forming process. It becomes more severe as the extrusion opening size is decreased. Therefore, understanding the phase segregation in micro-scale becomes more crucial. In addition, understanding the rheological characteristics of the semisolid powder flow is critical for the development of the SPP technique.

SPP is capable of precisely controlling the material composition, and thus may be applied to the fabrication of FGS. Potentials of SPP for the fabrication of FGSs are assessed by investigating graded ceramic-reinforced aluminum matrix composites.

1.2.1 Experimental Study on Viscosity and Phase Segregation of Al-Si Powders in the Semisolid State

This section focuses on the potential application of SPP in micro-scale part forming. The Al-Si binary system was chosen for its excellent performance in the wear resistance applications. Back extrusion experiments were carried out to study the rheological characteristics and phase segregation. The relationship was investigated between viscosity and phase segregation with important processing parameters including shear rate, extrusion rate, pre-compaction pressure, and heating time.

1.2.2 Functionally Graded Structure Fabrication with Semisolid Powder Processing

In this section, Al-Si-Cu and SiC powders were selected to form a two-layer FGS. The effects of the SiC reinforcement amount (20 wt% and 50 wt%) and SiC powder size (1200 mesh and 240 mesh) on the mechanical property and microstructures were investigated.

1.3 Dissertation Organization

The remainder of the dissertation is divided into three chapters. In chapter two, rheological characteristics and phase segregation in the micro-scale SPP are studied. In chapter three, investigation on the application of SPP in fabrication of FGS is performed. In the last chapter, a summary of the study is presented.

CHAPTER 2. EXPERIMENTAL STUDY OF VISCOSITY AND PHASE SEGREGATION OF AL-SI POWDERS IN THE SEMISOLID STATE

In this chapter, a set of back extrusion tests was performed to understand the flow characteristics of powders in the semisolid state. Design of experiment analysis was performed to understand the effects of process parameters, which includes pre-compaction pressure, shear rate, heating time and extrusion ratio, on the viscosity and phase segregation. In addition, a mathematical expression was developed to quantify the phase segregation.

2.1 Background on Semisolid Powder Processing

Processing of powder materials in the semisolid state has a rather short history [10, 11] compared with commonly practiced bulk material processing which started in the 1970s [6]. The semisolid bulk forming and semisolid powder processing are schematically compared in Fig. 1. SPP expanded the bulk semisolid forming by replacing bulk material with powders, which would provide 1) more flexible control of material composites by varying the amount, size and type of the powders; 2) less energy consumption and simpler processes because of the inherent microstructure refinement; and 3) better microstructure and mechanical properties of the final products.

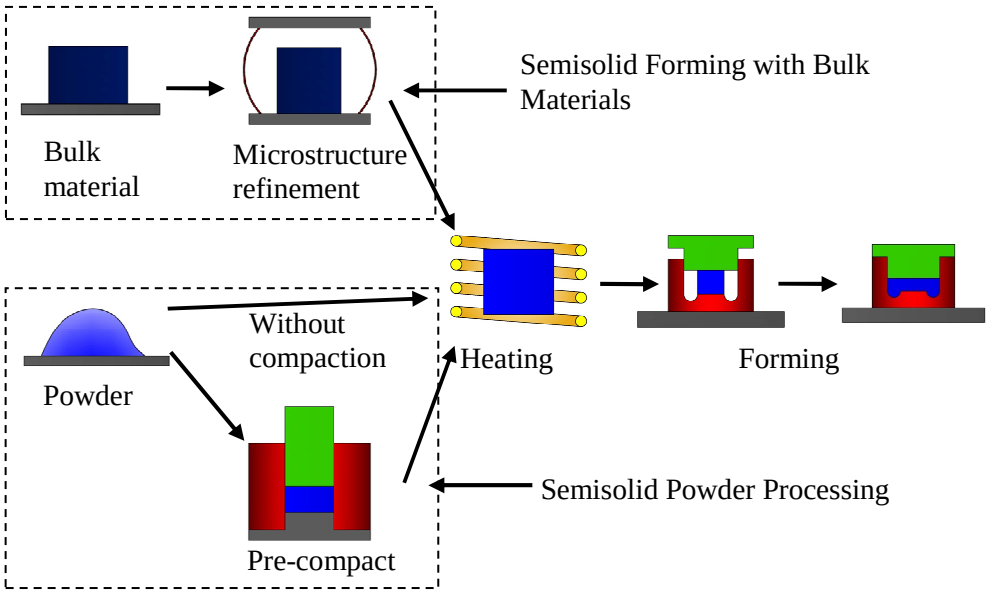

Fig. 1: Comparison between bulk semisolid forming and semisolid powder processing

A summary of various processing routes of SPP is shown in Fig. 2 [10-19]. In general, four basic steps are required: powder preparation, powder compaction, pre-heating and semisolid forming. Powder blends may be mixed either from at elemental or prealloyed powders. The powder compaction can take place at room temperature (cold pressing [15]) or at elevated temperatures (hot pressing [12, 18, 19]). The heating may be achieved by induction heating [18] or by direct furnace heating [12-14, 19]. Finally, at a designed temperature, the semisolid state powders are formed into near-net shape parts. Homogeneous and well-densified structure compacts were observed in macroscale parts [11-14]. Also, the mechanical properties of the parts produced by SPP were comparable to conventional forming methods [13, 15, 16, 18].

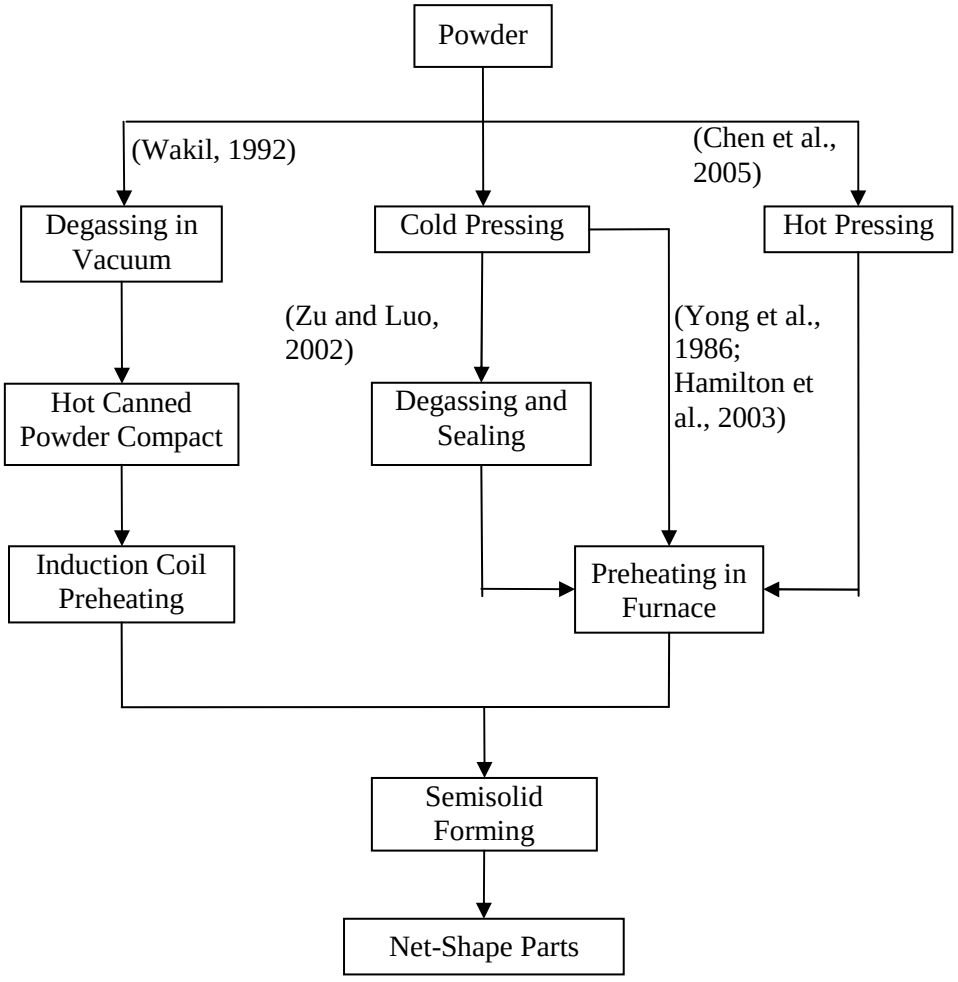

Fig. 2: Process routes of various semisolid powder processing

Researchers have investigated flow characteristics of bulk materials in the semisolid state by measuring viscosities. Various techniques such as concentric cylinder rheometer [20, 21], capillary viscometer [22], compression tests [23-25] and back extrusion [26-28] have been used. The back extrusion technique for viscosity measurement of semisolid materials is a newer development. The back extrusion process can be used for actual part fabrication, and therefore, the test conditions are similar to the actual process. Experimental

results indicated shear thinning behaviors of the bulk semisolid materials, i.e. the apparent viscosity decreased as the shear rate increased [27, 29-32]. As expected, apparent viscosity increased as the solid fraction of semisolid material increased [32-35].

The phase segregation during forming of semisolid materials is another important phenomenon that can influence the final part quality [36]. In the back extrusion experiments of bulk semisolid materials at macroscale, a higher liquid fraction was typically observed in the extruded region than the remaining region [28, 37, 38]. Effects of processing parameters including ram speed, extrusion opening and billet heating time on phase segregation were investigated [18, 28, 36, 39]. The phase segregation increased as the ram speed or the shear rate decreased [18, 28, 40]. Experiments also showed that phase segregation was eliminated when the shear rate increased to a certain level [36, 41]. In addition, it was speculated that the extrusion ratio affected phase segregation significantly [28, 41, 42]. Development of models that can predict the phase segregation of bulk semisolid material are also in progress [36, 38, 43, 44]. The modeling results demonstrated a strong correlation between the segregation behavior with the microstructure, permeability and liquid phase percolation velocity during extrusion of the bulk semisolid materials.

Past and current research on the semisolid processing shows a great potential for the technology to become a viable manufacturing route for micro/meso-size features. With powders as feedstock materials, the technology can exploit the advantages of powder metallurgy. However, no quantitative work has been performed on the flow behavior and

phase segregation of powders in the semisolid state at micro/meso-scale ranges (10-5000 μm).

2.2 Experimental Method

2.2.1 Materials and Equipments

Hypereutectic pre-alloyed Al-50Si powder (supplied by Ames Laboratory of US Department of Energy) was used in this study due to its potential applications for high wear resistant components [45]. The measured mean diameter and particle size distribution are summarized in Table 1, where d_{10}, d_{50} and d_{90} represent the 10^{th}, 50^{th} and 90^{th} percentiles of the diameter distribution. The microstructure of the original powder and phase diagram of Al-Si binary alloy system are shown in Fig. 3 and Fig. 4, respectively. The Al-50Si is composed of liquid and pure solid Si phase between 577°C and 1051°C, and therefore, a large window of operating temperature is provided.

Table 1: Size distribution of the initial Al-50Si powder

Mean size	*Powder Size (μm)*		
(μm)	d_{10}	d_{50}	d_{90}
16.96	9.55	15.53	25.69

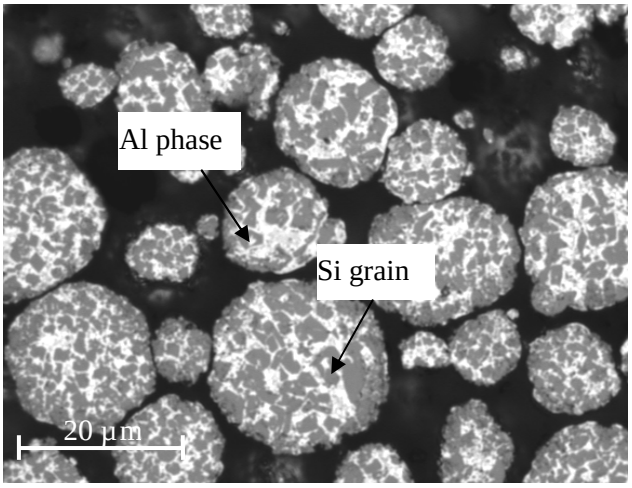

Fig. 3: Original Al-50Si powder used in the experiments

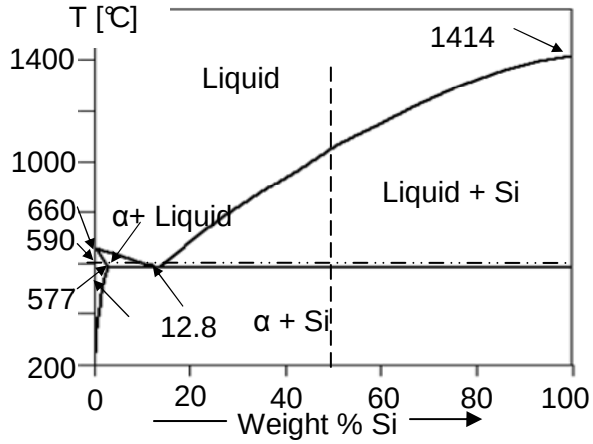

Fig. 4: Phase diagram of Al-Si binary alloy system

The experiments were carried out at 590°C at which temperature the solid fraction was 0.42 (calculated by ThermoCalc version 3.1). At 590°C, all of the Al (50 wt% of the total weight) and a limited amount of Si (8 wt% of the total weight) are melted. The Si volume fraction in the liquid phase is about 13%.

The microstructures of the samples were observed with an Optical Microscope (ZEISS, Model: Axiovert 200 M). Hardness of samples was measured by LECO LM247AT Micro Hardness Tester. Commercial software IQMaterial was used to analyze the microstructure of the samples. The Si phase, Al phase, porosity and the Si grain characteristics were analyzed.

2.2.2 Experimental Setup and Analysis Method

A back extrusion test has been employed to study the phase segregation of Al-Si powders in the semisolid state. As shown in Fig. 5, a fabricated die set is placed within the furnace (Applied Test System Inc, Series 3210) where the load and movement of upper ram are controlled and measured by the materials testing system (TestResources Inc, 800LE). Since the diameter of the container is fixed, the extrusion opening can be changed by varying the punch diameter. The experiment die set was first sprayed with Boron Nitride coating to prevent the reaction between the liquid state material and stainless steel die. The Al-Si powder was poured into the container and was compacted (or kept in a loosed state) before placing in the furnace. After the temperature reached the set point, it was held for a required heating period before the upper ram moved down at a designed velocity. The semisolid state powder (or powder compact) was pushed into the extrusion opening, forming a cup-shaped part. The final pressure applied in each experiment was set to 100 MPa.

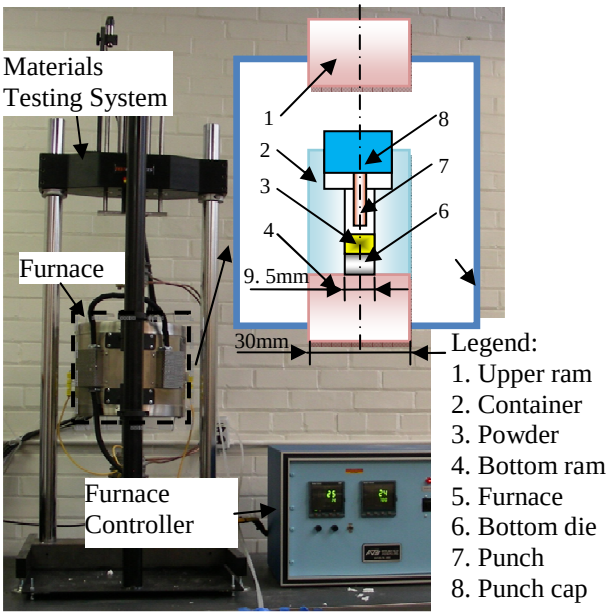

Fig. 5: Setup for back extrusion of semisolid powders

The actual temperature of the material was measured directly in a separate experiment. As shown in Fig. 6, a thermocouple was inserted into the powder material for direct temperature measurement. The heating curve selected for the experiments is shown in Fig. 7. The furnace was first heated up to 647 °C and held for 30 minutes to increase the heating rate of die set. After that, the set point of the furnace was set to 617 °C, which was approximately 27 °C higher than the target temperature to compensate for the temperature difference between the furnace and the die set. As seen in the figure, the temperature of the die set achieved 590 °C after heated by 72 minutes and it was relatively stable after that.

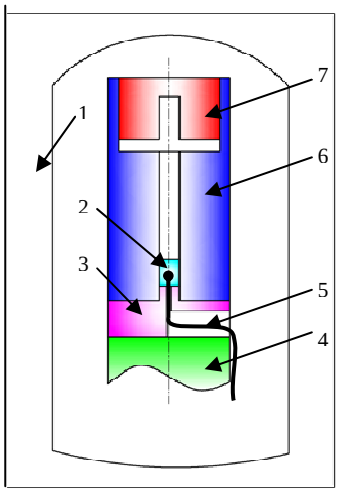

Legend:

1. Furnace
2. Powder
3. Bottom die
4. Bottom ram
5. Thermocouple
6. Container
7. Punch cap

Fig. 6: Temperature testing die set mechanism

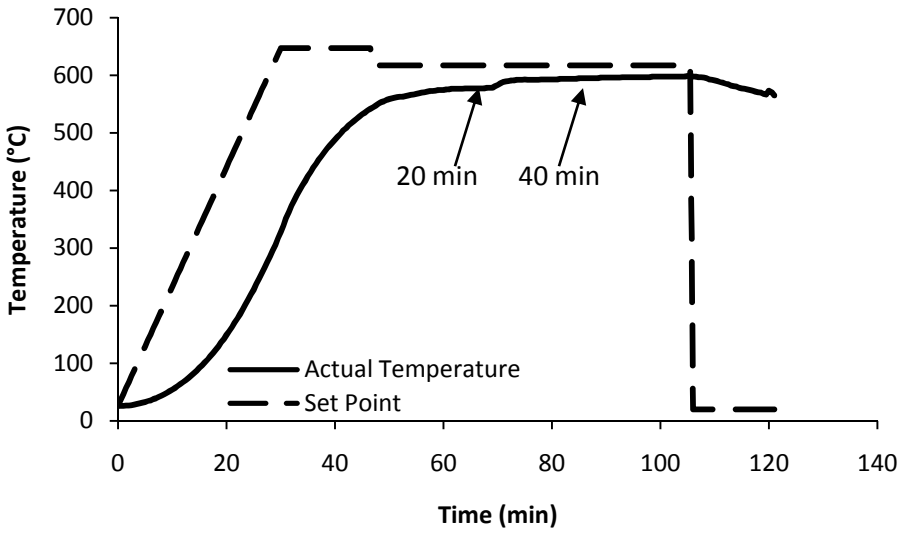

Fig. 7: Heating curve in the back extrusion experiments

A design of experiments analysis was performed to understand the effects of process parameters on the viscosity and phase segregation. Four experimental parameters including shear rate, pre-compaction pressure, extrusion ratio and heating time were selected.

Commercial statistical software, JMP, was utilized to produce the experiment design and to perform data analysis. The experimental array and results are summarized in Table 2.

Table 2: Experiment array and result

	Parameters				*Results*	
No.	λ	$\dot{\gamma_{av}}$*(1/s)*	*P (MPa)*	*t (min)*	η_{app}*(Ns/m^2)*	*ps*
1	3.27273	4	0	20	44068.9	0.248
2	3.27273	4	0	40	19342.7	0.304
3	6.12268	100	0	20	344.7	0.245
4	6.12268	100	50	20	308.3	0.199
5	6.12268	4	100	40	2881.8	0.291
6	6.12268	20	50	40	1012.6	0.307
7	3.27273	20	100	20	7239.2	0.232
8	2.28571	4	50	20	71235.3	0.230
9	2.28571	20	100	20	8059.3	0.270
10	2.28571	20	0	40	4183.5	0.240
11	3.27273	100	50	40	1156.1	0.210
12	2.28571	100	100	40	1296.4	0.218

Note: λ is extrusion ratio, $\dot{\gamma_{av}}$ is shear rate, *P* is pre-compaction pressure and *t* is heating time.

2.2.3 Calculation of Viscosity and Phase Segregation

In the back extrusion experiment, the apparent viscosity and shear rate can be calculated by a set of equations developed by Loue et al. [26]:

$$\eta_{app} = \frac{1}{2\pi\lambda C_1 V_p} \cdot \frac{dF}{dt} \quad \textbf{(1)}$$

$$\dot{\gamma_{av}} = \frac{C_1\left[ln\left(\frac{-C_1}{2C_2R_cR_p}\right) - 1\right] - C_2\left(R_c^2 + R_p^2\right)}{R_c - R_p} \quad \textbf{(2)}$$

where *dF/dt* is the load change rate; R_c and R_p are the radii of the container and punch, respectively; V_p is the punch velocity; λ is the extrusion ratio. λ, C_1, C_2 are given in the following equations:

$$\lambda = \frac{{R_c}^2}{{R_c}^2 - {R_p}^2} \tag{3}$$

$$C_1 = \frac{1}{\ln\left(\frac{R_p}{R_c}\right)} \cdot \left(C_2 \cdot \left({R_c}^2 - {R_p}^2\right) - V_p\right) \tag{4}$$

$$C_2 = \frac{V_p}{\left({R_c}^2 - {R_p}^2\right) - \left({R_c}^2 + {R_p}^2\right)\ln\left(\frac{R_p}{R_c}\right)} \tag{5}$$

Apparent viscosity and shear rate can be obtained from geometric dimensions (R_c and R_p), punch velocity (V_p) and rate of force change (*dF/dt*).

In this paper, a simple mathematical approach to quantify the severity of phase segregation based on 2-D images is developed. The deviation of the element content from its original content at a local position *i* can be defined as:

$$ps_i = |c_i - c_0| \tag{6}$$

where ps_i is the measure of phase segregation at local position, c_i is the element fraction (e.g. Si fraction) at a position *i*, and c_0 is the initial element fraction. Therefore, the phase segregation over the total cross sectional area can be defined as:

$$ps = \frac{1}{A}\int_A ps_i dA \tag{7}$$

where *A* is the total area of interest. Equation (7) can be discretisized to calculate phase segregation over finite number of elements with equal size area:

$$ps = \frac{1}{A}\sum_{i=1}^{N} ps_i\, A_i = \frac{1}{N}\sum_{i=1}^{N} |c_i - c_0| \quad \textbf{(8)}$$

where *N* is the total number of discretisized areas that phase segregation is measured.

2.3 Results and Discussion

2.3.1 Microstructure Analysis

Typical microstructures at various locations of an extruded part are shown in Fig. 8. Representative microstructures of positions A through G were selected from run #11 in Table 2. In general, connected solid structures were observed under the punch. The wall section (A through D) showed disconnected original particles. Completely different Si grain shapes were observed at location A, where the Si grains were mostly needle shape. The Si grains in other areas were spherically shaped or inter-connected, irregularly shaped. The distinct difference in the shapes of the Si phase indicated different formation processes at respective locations. The microstructure of Al-Si shown at position A is typical of the eutectic structure, where the Si phase is fibrous (needle shape). Therefore, this structure resulted from the solidification of the liquid phase containing liquid Al and eutectic composition. The Si volume fraction measured at location A was around 16%, which is consistent with the calculated value of 13%. At other locations, the Si grains became larger during the heating process. Depending on the pressure applied during the forming process, either inter-connected irregular Si grains (E, F and G) or Si trapped in disconnected particles were formed.

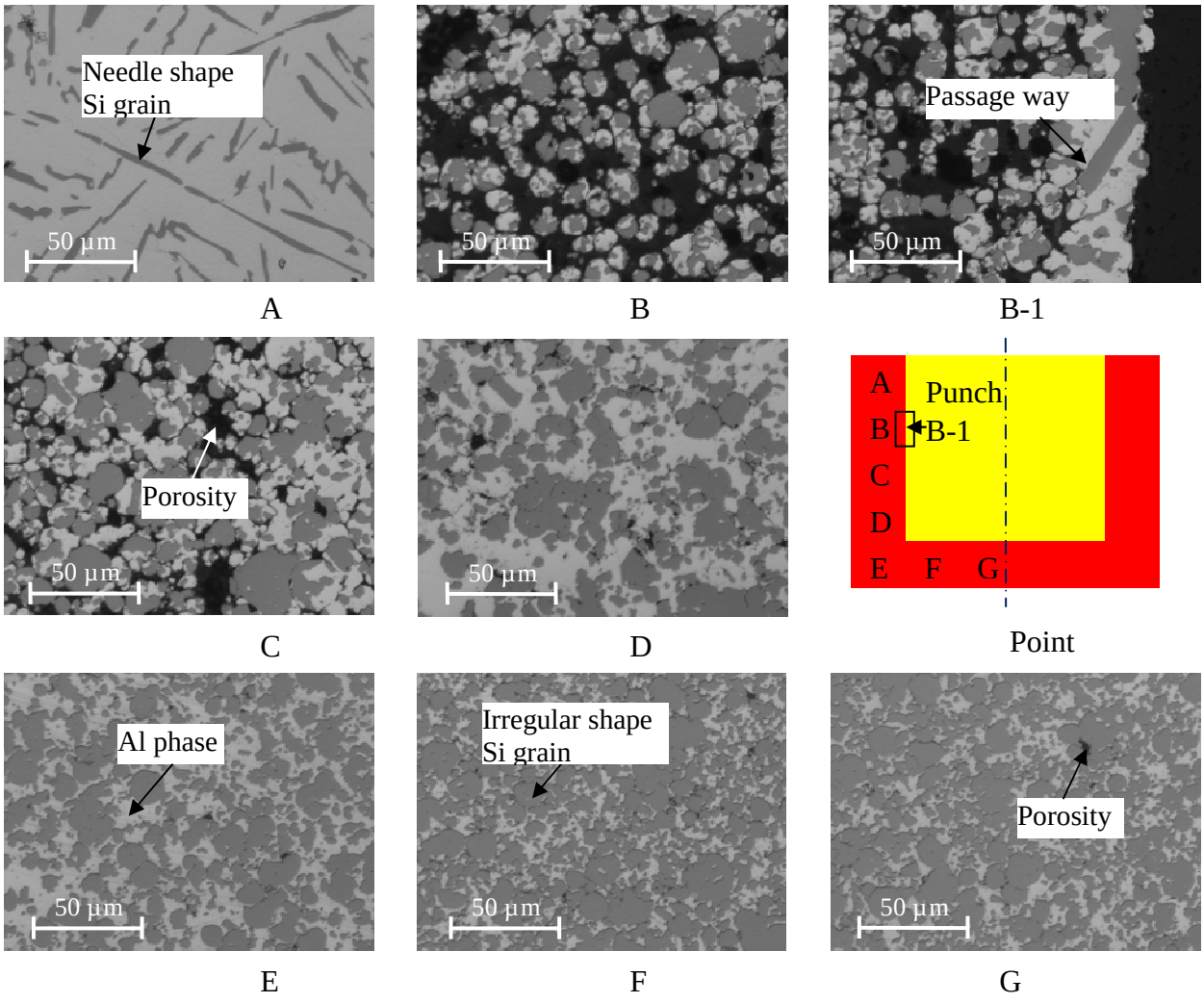

Fig. 8: Microstructures at different locations of a back extruded part (run #11 in Table 2)

The highest Si concentrations (a mean volume fraction of 0.73) were found in locations F and G. Since the majority of Si is in solid state at 590°C, the liquid phase was squeezed into the extrusion opening during the forming process. Therefore, locations F and G were left with high remnant Si concentrations. From the microstructural observations, it was speculated that liquid phase separated from the solid phase during the extrusion process and traveled though the wall section along the punch edge. As shown in Fig. 8 B-1, former

liquid phase was observed along the edges of the punch indicating a passage way for the liquid phase. Thus, the liquid phase does not homogeneously flow into and through the wall section. Rather, it finds a minimal resistant passage along the punch edge, and ends up at the top of the wall (location A).

2.3.2 Viscosity

The viscosity calculation requires force change rate measurement (dF/dt). A typical force-displacement curve is shown in Fig. 9. During the extrusion process, the structure of the semisolid material also evolves. Initially, the material is at a relatively loose state. As the material is squeezed, the powders form an inter-connecting structure. Therefore, overall the structure becomes more rigid during the extrusion, as indicated by the steep increase in the slope of the force-displacement curve. For the calculation of viscosity, the initial dF/dt response was used.

A design of experiments approach was employed to determine the statistically significant factors. Analysis of variance result is summarized in Table 3. The p-value indicates the significance of each parameter. The factor is significant when p-value is less than 0.05. The statistical analysis shows that the shear rate, extrusion ratio and heating time are statistically significant factors influencing the viscosity of powder in the semisolid state. The pre-compaction pressure was not a significant factor for the range covered in this study.

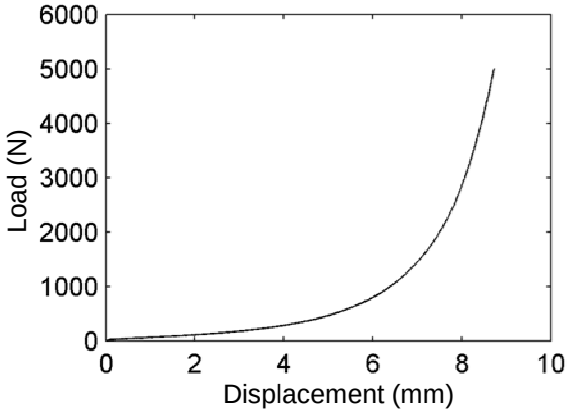

Fig. 9: Typical force-displacement during back extrusion of semisolid Al-50Si powders (run #1 in Table 2)

Table 3: Effect test result for viscosity

Source	*DF*	*Sum of Squares*	*F Ratio*	*P-value*
Heating time	1	8.56×10^{8}	11.29	0.0283
Extrusion Ratio	2	1.07×10^{9}	7.03	0.0490
Pre-compaction Pressure	2	7.71×10^{8}	5.08	0.0769
Shear Rate	2	2.51×10^{9}	16.57	0.0116

The effects of each parameter on the apparent viscosity are reported in Fig. 10. The viscosity decreased as shear rate increased, which showed that the powder material in the semisolid state behaved like a shear thinning material. Furthermore, the viscosity decreased with the increase of extrusion ratio. When the size of extrusion opening decreased (i.e., as the extrusion ratio increased), it became more difficult for the semisolid state particles to pass through the opening. Consequently, more liquid phase passed through the extrusion opening, which resulted in lower viscosity for smaller openings. Higher phase segregation observed at

smaller opening supports the speculation (see Fig. 12). The apparent viscosity also decreased as the heating time increased. The mean size of the Si grains grew 140% as the heating time increased from 20 to 40 minutes. For a given extrusion opening, liquid phase separation is more likely to occur for the structures with larger Si grains causing the viscosity to drop.

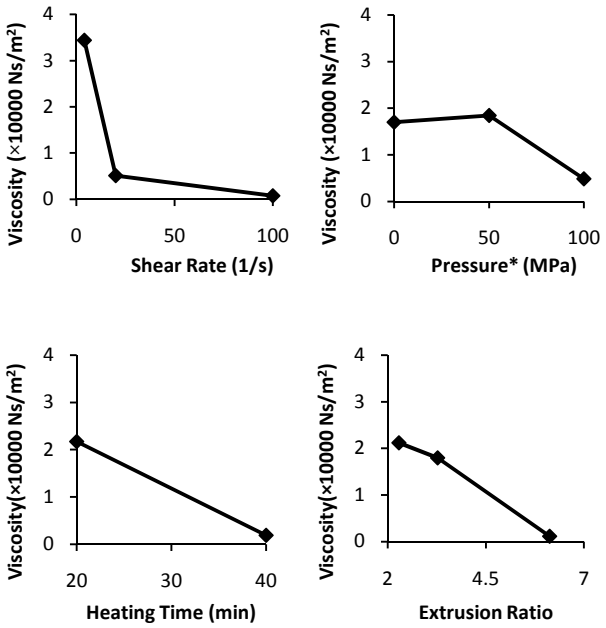

Fig. 10: Mean values of viscosity at different parameter levels.

*: Pre-compaction pressure

2.3.3 Phase Segregation

Analysis of variance results for the phase segregation are summarized in Table 4. None of the parameters had statistically significant effect on the phase segregation for the parameter range selected in this work. The absolute phase segregation values, however, were quite large at an average value of 0.25. The distribution of Si fraction is graphically illustrated in Fig. 11, which shows the severity of phase segregation. Fig. 11(a) and (b)

compare the effect of shear rate on the phase segregation – at higher shear rate, the magnitude of phase segregation is smaller.

Table 4: Effect test result for phase segregation

Source	*DF*	*Sum of Squares*	*F Ratio*	*P-value*
Heating time	1	0.0018	2.01	0.2295
Extrusion Ratio	2	0.0027	1.53	0.3199
Pre-compaction Pressure	2	0.0005	0.31	0.7506
Shear Rate	2	0.0065	3.62	0.1267

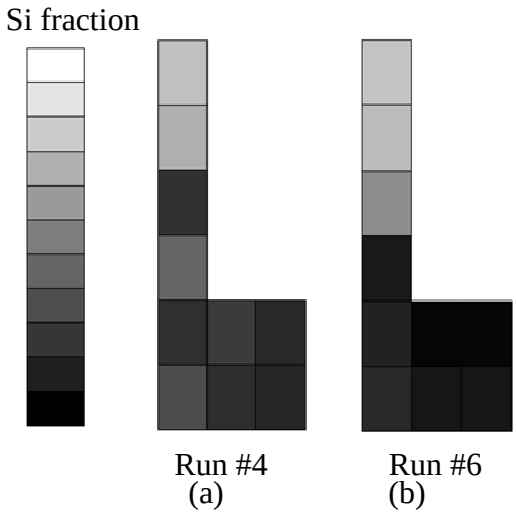

Fig. 11: Silicon fraction at different positions in the samples; part (a) is fabricated with λ=6.12 and $\dot{\gamma}_{av}$=100; (b) λ=6.12 and $\dot{\gamma}_{av}$=20; Darker area and bright area mean either high Si concentration or Al concentration, respectively.

The detailed plots for each factor are shown in Fig. 12. As the shear rate increased, the phase segregation decreased. The observation is also in agreement with results for bulk semisolid forming [28]. At higher shear rates, it is more likely that both the liquid and solid

phases flow simultaneously resulting in more homogeneous microstructure. At extremely low shear rate, severe liquid phase separation was observed in prior experiments conducted by the authors. The liquid phase traveled through the particles, leaving the solid phase under the punch. The phase segregation increased with the increase of extrusion ratio. With thinner wall sections (i.e., higher extrusion ratio), the flow of the solid phase will be severely restricted, and therefore, greater phase segregation will occur.

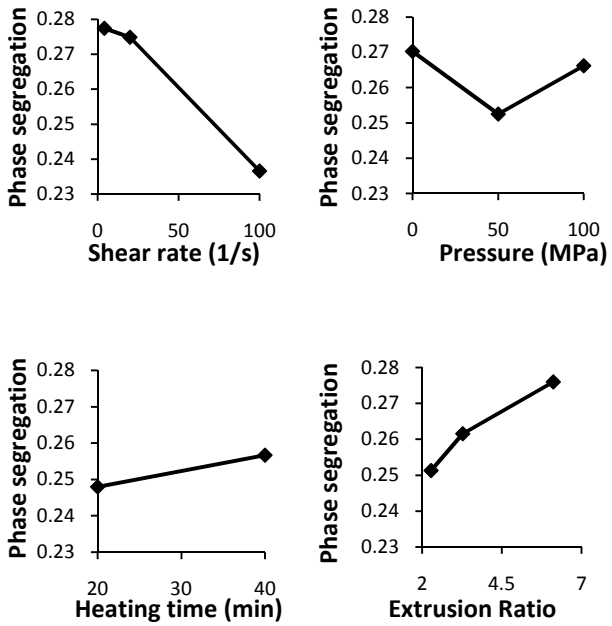

Fig. 12: Mean value of phase segregation at different parameter levels

2.3.4 Characteristics of Semisolid Powder Flow

A typical load-displacement curve of back-extrusion test is shown in Fig. 13. The response has been divided into three zones since the rate of change in load-displacement curve indicates structural evolution according to Eqn. (1). The force increased very slowly in Zone 1. After a non-linear increase in Zone 2, a sharp, linear increase in the force is

observed in Zone 3. To observe the microstructures at each stage, three additional experiments were performed as shown in Table 5. The first experiment was done to examine the initial status of powders just after heating (before forming). The other two experiments were performed to study the microstructures of the parts at the end of each zone, so that detailed information of the semisolid flow may be obtained.

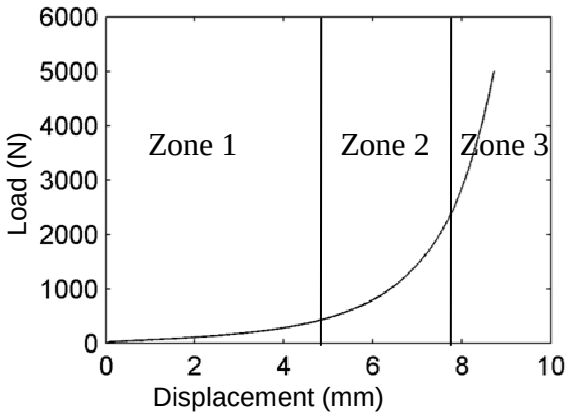

Fig. 13: Typical force-displacement during back extrusion of semisolid Al-50Si powders (run #1 in Table 2)

Table 5: Additional experiments for characterization of semisolid powder flow

	Parameters				
No.	λ	$\dot{\gamma}_{av}$*(1/s)*	*P (MPa)*	*t (min)*	F_{max}*(N)*
13	0	0	50	40	0
14	3.27273	100	50	40	500
15	3.27273	100	50	40	2500

Note: F_{max} is the maximum force in the forming process.

The microstructure of the powders just after heating (Exp. No. 13) is shown in Fig. 14. Compared with the initial powder (see Fig. 3), the Si grains grew from 3.02 μm to 10.39 μm, aggregated from a set of small discrete Si grains into a larger Si core. No agglomeration

of powders or liquid phase was found in the compact. The structure of the powder compact can be regarded as a loosed stacked compact, with over 50% porosity.

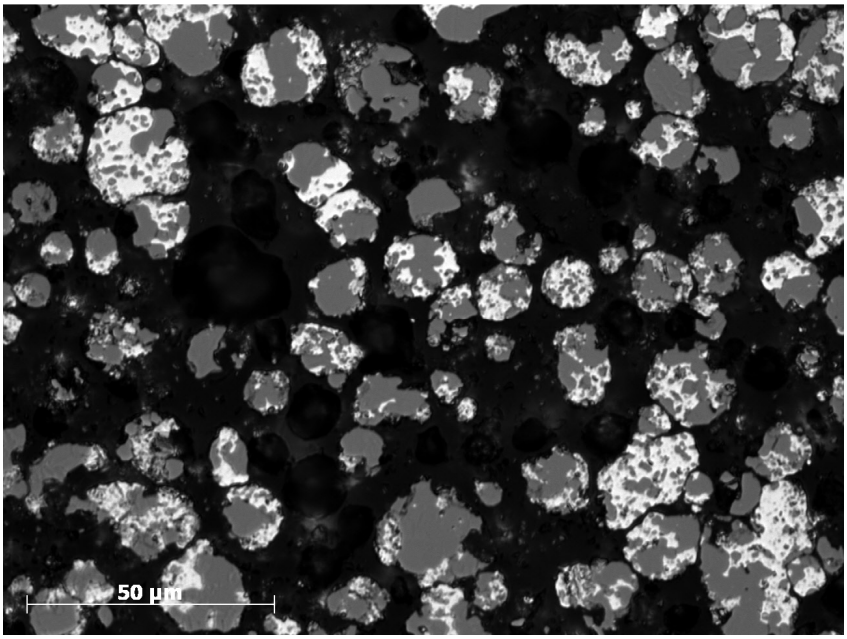

Fig. 14: Powders just after heating (run #13 in Table 5)

Fig. 15, Fig. 16 and Fig. 17 show the comparison of microstructures obtained from Exp. 14, Exp. 15 and Exp. 11, which were stopped at the end of each zone. The experiments were stopped at the corresponding load of 500 N (7.7 MPa), 2500 N (38.5 MPa) and 6500 N (100 MPa), and are shown in respective columns.

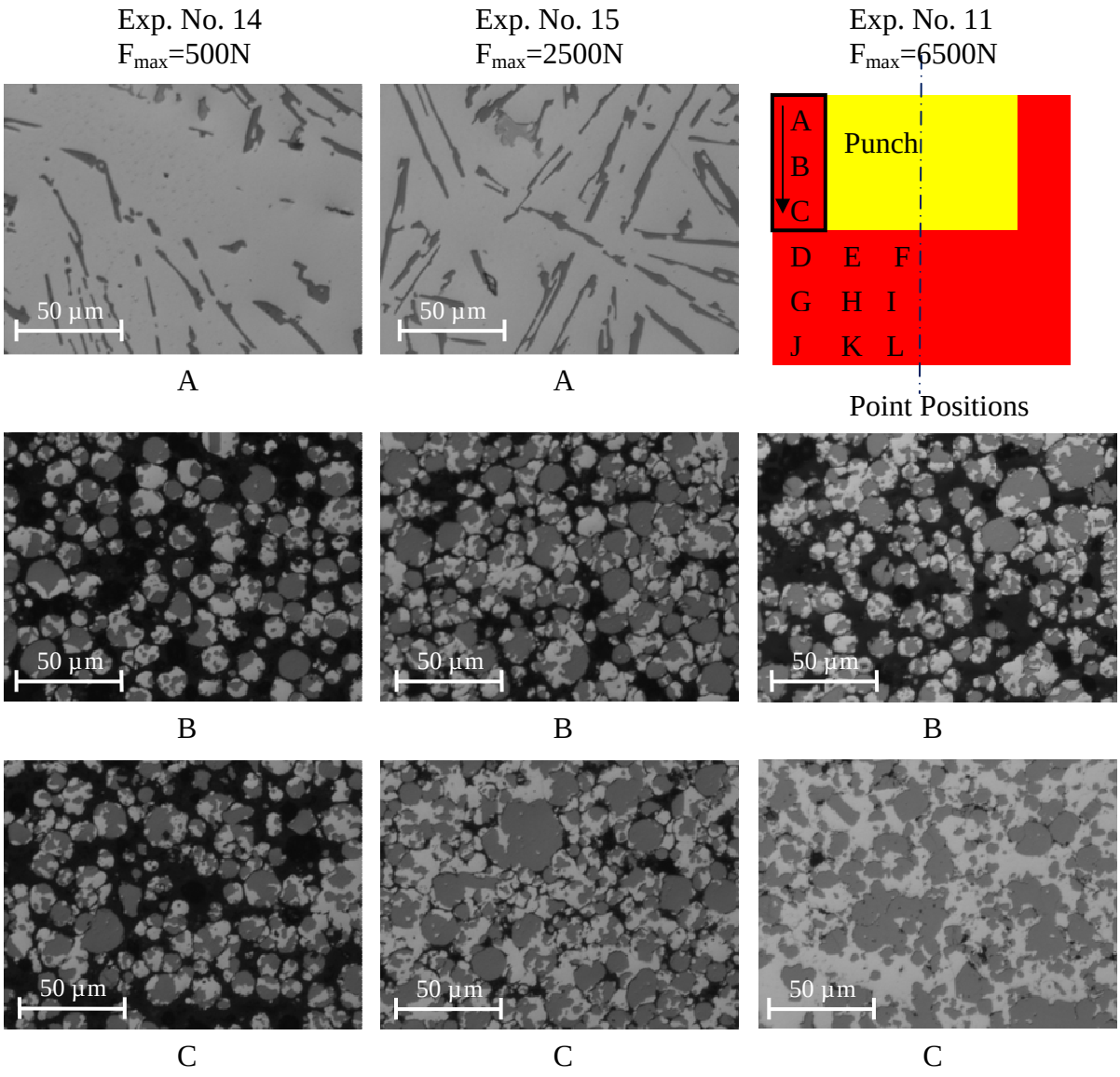

Fig. 15: Comparison of microstructure of parts obtained from different maximum pressure (position A to C). Note position A for Exp. 11 can be found in Fig. 8, in which the microstructure was similar to position A in Exp. 14 and Exp. 15.

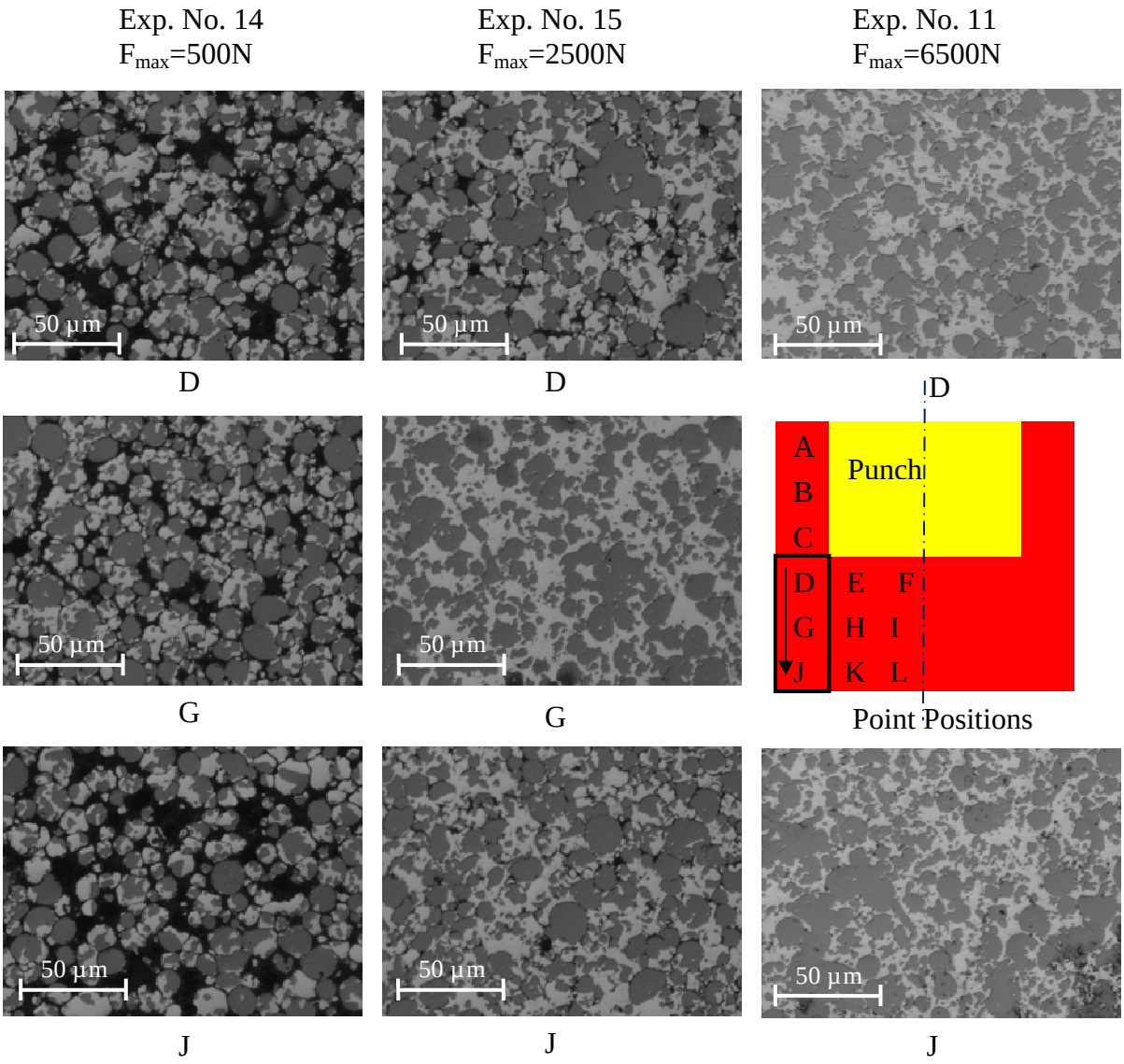

Fig. 16: Comparison of microstructure of parts obtained from different maximum pressure (position D, G, J)

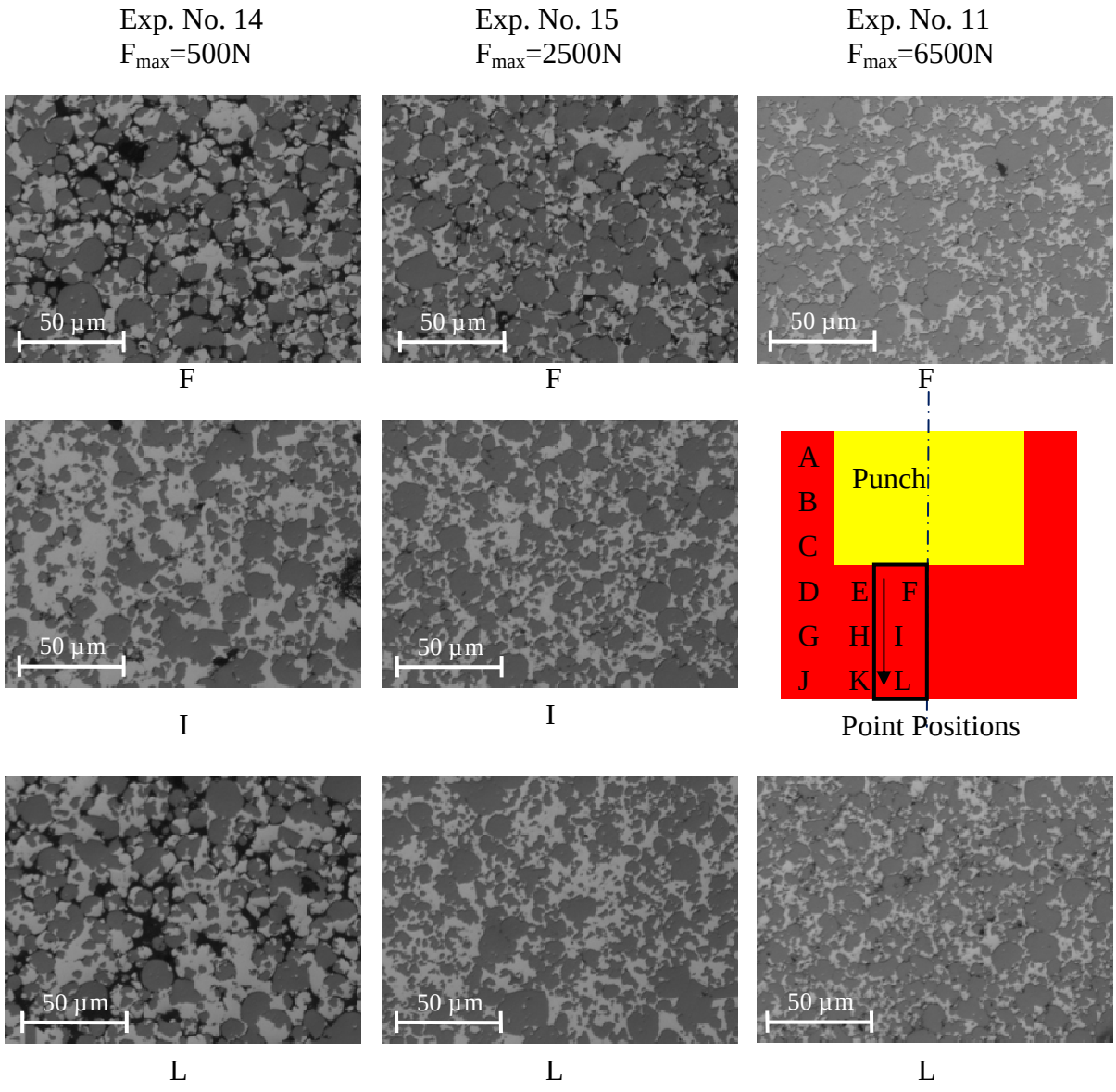

Fig. 17: Comparison of microstructure of parts obtained from different maximum pressure (position F, I, L)

First, microstructures of a part from Exp. 14 (with the maximum forming force of 500 N) were shown in the first column in Fig. 15, Fig. 16 and Fig. 17. As shown in Fig. 15, position A was filled with liquid when the force was only 500 N. Hence, severe phase

segregation occurred in the very early stage in the extrusion. The microstructures at positions B and C were very similar to that of powders just after heating (see Fig. 14). It implied that these were the powders from near the wall, at the top the powder compact. Furthermore, it can be found that, from the first column in Fig. 16 and Fig. 17, the solid Si grains were compacted together and the porosity decreased compared with the initial powder compact when the forming force achieved 500 N.

When the force increased from 500N to 2500 N, the powder compact was further compacted. As shown in column 2 in Fig. 16 and Fig. 17, the porosity of positions beneath the punch area (D-L) decreased significantly, compared with that in column 1. In Fig. 17 F, I and L, solid Si grains started to deform and bond together, forming an inter-connected structure. Also, at position C (Fig. 15), the microstructure at the opening of the gap was a uniform mixture (although with some porosity) of the solid Si grains and Al-Si eutectic phase. This indicated that the uniform semisolid mixture started to enter the small gap at the end of Zone 2.

At the end of Zone 3, because of the small travel distance (approximately 2 mm), the microstructures are similar to that at the end of zone two. However, it is obvious that the further porosity decreased, and the part reached nearly full density at most positions beneath the punch.

In summary, the semisolid powder flow in the forming process can be summarized to be:

1. Preheating: the Al-50Si powders were heated to semisolid state, containing about 60% of the liquid phase. The particles were distributed evenly in the compact, with liquid material surrounding the Si grains.
2. Zone 1: In this stage, liquid phase segregation mainly occurs and the overall structure is still porous. The particles still retain their original shape.
3. Zone 2: The powders started to agglomerate and formed interconnected structure. The force increased sharply and non-linearly. At the end of this stage, nearly no porosity was observed beneath the punch. The load-displacement showed a transient behavior because the structure entering the channel evolved from loose particles to mixture of liquid phase and interconnected solid phase.
4. Zone 3: In this stage, a linear increase in the load was observed as interconnected structure entered the channel area. However, at this state, it is really difficult for the Si grains to deform, because the strength of Si grains is very high, which result in the high force increase rate. At the end of this zone, the porosity beneath the punch almost reached zero.

2.4 Conclusion

The flow behavior and phase segregation of Al-Si alloy powders in the semisolid state were studied for the development of novel SPP for micro parts fabrication. The effects of shear rate, extrusion ratio, heating time and pre-compaction pressure on microstructures, viscosity and phase segregation were investigated using back extrusion experiments.

Overall, a shear thinning behavior was observed for powders flowing in the semisolid state. The shear rate, extrusion ratio and heating time were found to be statistically significant factors affecting the viscosity. As the size of the extrusion opening decreased to 400 µm, the flow of semisolid powders were severely affected, and resulting microstructures showed significant phase segregation. Typical phase segregation amount observed for this study was *ps* value of 25% (from Eqn. (8)). At smaller extrusion openings, entrapped liquid phase within the particles had a tendency to separate from the original structure, leaving behind the solid phase contents, and travelling through the thin wall section. This resulted in lowering of apparent viscosity and increasing of phase segregation at smaller extrusion openings. The phase segregation also decreased with increasing shear rate. To minimize phase segregation at micro/meso-length scales, higher punch speed, shorter heating time and smaller extrusion ratio are recommended. It was also observed that phase segregation and viscosity were not strongly influenced by the pre-compaction pressure range (0-100MPa) covered in this study.

The semisolid powder flow may be divided into three stages. Severe phase segregation occurred in the first stage, even when the force is low.

The potential of processing materials in the semisolid state is very promising. Replacing bulk materials with powdered materials may add a new dimension to the technique by allowing tailoring of material properties. In this study, two fundamental aspects, viscosity and phase segregation behavior of the SPP was investigated for application in micro/meso-

manufacturing. To fully develop the technique, more in depth understanding of the process parameters and underlying physics is needed.

2.5 Future Work

Future work will focus on the understanding of the semisolid powder processing by computational simulation. The simulation of semisolid powder processing requires a model that can not only predict the movement of fluid and solid particles, but also capture the phase segregation for application in micromanufacturing. The model developed will be finally implemented into the flow modeling.

The most important purpose of the simulation is to study the effects of the forming velocity, channel size, solid fraction and particle size on the phase segregation. The schematic view of the possible simulation geometry is shown in Fig. 18. Phase segregation in the SPP may be induced by the pressure gradient due to outside force or geometry change. When the semisolid powder flow is pushed into the small channel, phase segregation will happen. The model governing phase segregation is expected to be implemented by discrete element method (MFIX DEM model). Also, experiments for matching the simulation results will be performed.

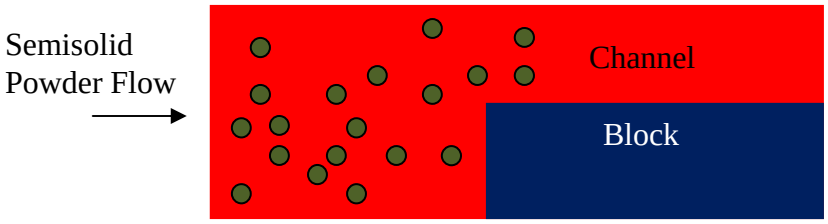

Fig. 18: Schematic view of the simulation geometry

CHAPTER 3. FABRICATION OF FUNCTIONALLY GRADED STRUCTURES BY SEMISOLID POWDER PROCESSING

3.1 Introduction

Functionally graded structure (FGS) materials exhibit change of material properties form one surface to another [46]. The potential application of FGSs was first recognized in the work of Bever and Duwez in 1972 [47]. FGS with varying mechanical, electronic or thermal properties, is attractive in many areas because of their capability of reducing in-plane and transverse stresses, decreasing residual stress, and improving mechanical/electrical properties [48]. However, current fabrication methods are not able to satisfy the increasing demand for the FGS materials.

Semisolid Powder Processing (SPP) exploits metallic powders in the semisolid or mushy state (i.e., between the solidus and liquidus temperature of an alloy system). SPP combines the concepts of powder metallurgy (P/M) and bulk semisolid processing techniques inheriting their advantages. This study investigates the potential of SPP for producing FGSs. Powders may be mixed to tailor the properties of a material, while a final part is formed during the process.

3.2 Literature Review

Different fabrication methods for FGSs are briefly reviewed in this section. Their advantages and disadvantages are presented. Surface coating methods including PVD [49], CVD [50], thermal spraying [51] and laser cladding [52] are capable of producing thin layer

coatings with promising mechanical properties and microstructures. However, poor bonding, coating porosity, cohesive strength expansion, and residual stress of the coating might lower the product quality[53]. In addition, coating methods are limited to vary the composition on the surfaces.

Powder metallurgy (P/M) [54, 55], casting [56-59] and infiltration [60-63] have been used for bulk FGS fabrication. Slip casting and centrifugal casting can produce FGS with high density [57, 64, 65]. However, post-processing is always required to reduce distortion and shrinkage of the parts. Also, the composition is affected by the gravitational force. P/M is capable of sintering FGS with highly controlled composition. Nevertheless, it often suffers from sintering imbalance and requires a complex green compact [55]. Percolation of ceramic powders would produce inevitable porosity in P/M process [66, 67]. Moreover, P/M is not applicable when the melting temperature of the metal and sintering temperature are significantly different [60]. For infiltration-based methods, inter-connected pores may not be possible when ceramic fraction is high (higher than 65 vol%) [60, 68]. Hence, liquid phase is not able to infiltrate into the closed or half closed pores, resulting in high porosity of the parts. A qualitative comparison of the processes for the manufacturing of FGSs is summarized in Table 6.

Table 6: Comparison of fabrication processes of FGS [53, 56, 69-71]

Process	Initial Cost	Composite Control	Efficiency
Surface Methods (CVD, PVD, Thermal spraying, laser cladding)	High	Medium	Low
Slip Casting	Low	Medium	Medium
Centrifugal Casting	Low	Low	High
P/M	Low	High	High
SPP	Low	High	High

Semisolid state materials have been used to produce ceramic and metal matrix composites, which show the potential to produce bulk FGSs with high efficiency, low cost and high compositional control with promising microstructure. Zu et al. and Luo et al. [13, 16] demonstrated that the process is capable of processing ceramic particulate reinforced metal matrix composites with fine microstructure. Hybrid composite reinforced by both ceramic and graphite was also produced by SPP and the mechanical properties of the parts were promising [19]. Other materials including Al-Si [12, 17], Al-Ti [72, 73] and Al-Mg [10, 11] parts with good mechanical properties [72] were fabricated through SPP. In this paper, SPP method was applied to the fabrication of FGS for the first time.

3.3 Experimental Method

In this study, a two-layer FGS with one layer reinforced by SiC particles was fabricated by SPP. Different amount and size of SiC particles were added and their effects on the microstructure and mechanical properties were investigated.

The experimental setup is shown in Fig. 5. The fabricated die set is placed within the furnace (Applied Test System Inc, Series 3210) where the load and movement of upper ram are controlled and measured by the materials testing system (TestResources Inc, 800LE). The powder was directly poured into the container. After the temperature reached the set point, it was held for a required heating period before the upper ram moved down at a designed velocity. 50 MPa pressure was loaded and held for 30 seconds. The velocity of the punch was set to be 0.065 mm/s.

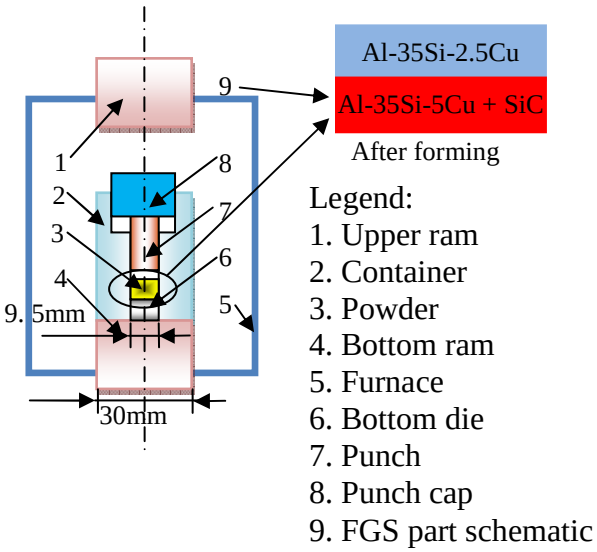

Fig. 19: Die set for semisolid powder processing

In this study, Al-Si-Cu system powders were chosen as the matrix material and SiC powders were used as a reinforcement composition. The liquid fractions of some Al-Si-Cu alloy system at different temperatures are listed in Table 7.

Table 7: Dependence of liquid fraction on temperature for some Al-Si-Cu alloys [74]

	Al-25Si-5Cu wt% liquid fraction	Al-35Si-2.5Cu wt% liquid fraction	Al-35Si-5Cu wt% liquid fraction
530 °C	9	0	9
540 °C	12	0	16
550 °C	24	4	25
560 °C	42	14	47
565 °C	61	20	72

In the experiment, functionally graded structure with two layers of different materials was fabricated, i.e. mixed SiC and Al-Si-Cu layer and pure Al-Si-Cu layer. Since SiC powder has high melting temperature, it will remain in the solid phase during the forming process. To make sure the liquid fraction is kept at a reasonable level in both layers, Al-

35Si-2.5Cu and Al-35Si-5Cu were chosen and the target temperature was set to 565 °C. As shown in Table 7, the solid fraction of Al-35Si-2.5Cu and Al-35Si-5Cu were 20% and 72%, respectively. Al-35Si-5Cu is mixed with SiC particles, which will lower the liquid fraction in the reinforced layer. The powders were blended by SPEX 8000M mixer with Al-50Si (supplied by AmesLab DOE, 20-45 μm), Al (supplied by AmesLab DOE, 20-45 μm) and Cu (supplied by AEE.inc, 1-5 μm).

Four experiments (Table 8) were performed to understand the effect of SiC particle size and amount on the microstructure and mechanical properties. The microstructures of the samples were observed with the optical microscope (Zeiss, Axiovert 200 M) and SEM (JEOL JSM-606LV). Hardness of samples was measured by LECO LM247AT Micro Hardness Tester.

Table 8: Experimental settings for FGS fabrication

Fixed Experimental Parameters		
Top Layer Material	Al-35Si-2.5Cu	
Bottom Layer Base Material	Al-35Si-5Cu	
Reinforcement Particle	SiC	
Temperature	565°C	
Forming Pressure	50 MPa	
Pressure Load Time	30 s	
Variable Experimental Parameters (Bottom layer SiC particle amount and size)		
Exp. No.	SiC amount (%)	SiC powder size (mesh/μm)
1	20	240/45
2	20	1200/12.5
3	50	240/45
4	50	1200/12.5

A separate experiment was performed to validate the actual temperature of the material during the forming process. To reduce the overall heating time, heating cycling curve as shown in Fig. 20 has been selected. The solid line shows the control temperature and dashed line is the actual temperature measured inside the powders. The furnace temperature goes up to 610 °C in the first 30 minutes and then is held for 20 minutes. After that, the control temperature is lowered to 580. As shown in the figure, about 30 minutes after the furnace set point had reached 580 °C the temperature of materials achieved 565 °C.

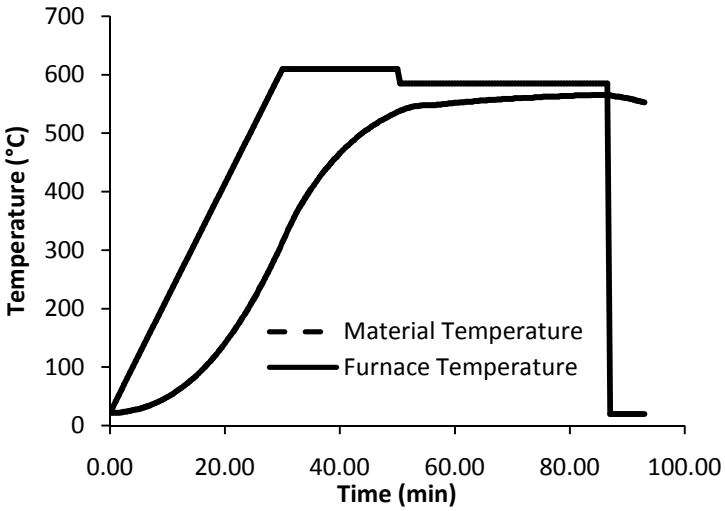

Fig. 20: Thermal cycle in the experiments

3.4 Results and Discussion

3.4.1 Microstructure of the FGS

The typical microstructure of the top layer (Al-35Si-2.5Cu) is shown in Fig. 21. Well densified layer with fine microstructures was formed in all the parts. The Si phase and Al

phase shown in the image were solid during the forming process. Some big pores were observed within the Al and Si solid phases, where the liquid was unable to penetrate.

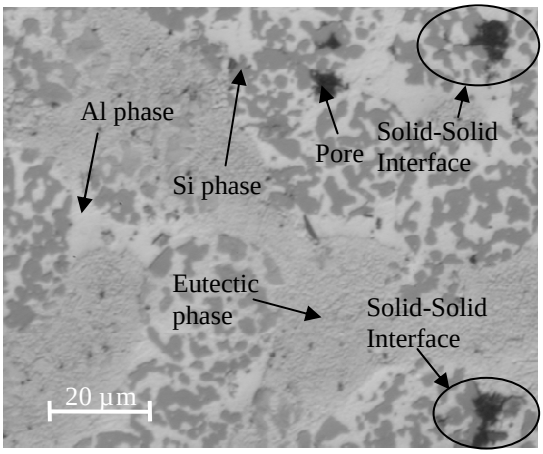

Fig. 21: Optical image of typical microstructure of the Al-35Si-2.5Cu layer (from Exp. No. 2)

The bottom layers (Al-35Si-5Cu + SiC) showed distinctly different microstructures with different SiC reinforcement particles sizes. As shown in Fig. 22 (a), when the size of SiC is large (45 μm), the SiC particles bonded well with the Al-Si-Cu, and high density composite was achieved. On the other hand, when the size of SiC is small (12.5 μm), the metal particles remained in their initial spherical shape and agglomeration of SiC particles were observed (Fig. 22 (b)). When the SiC particle was larger than the metal powders, it was surrounded by the small metal powders. Therefore, when the temperature achieved 565 °C, the liquid phase metal bonded with the SiC particles resulting in high density parts. When the SiC particle was smaller than the metal powders, the metal particles were isolated by the SiC particles. This is verified from the SEM image in Fig. 23 showing metal particles surrounded by small SiC particles. Because of the isolation among Al-Si, Al and Cu powders, little liquid state material was formed during the forming process due to limited

reaction among the metal powders. Therefore, a part with high porosity and low strength was formed, directly resulting in cracking of the part.

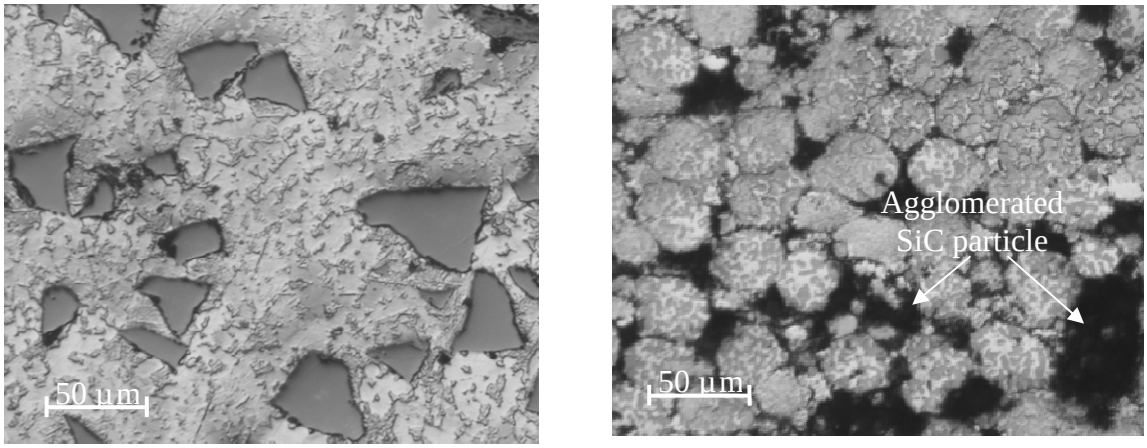

(a) (b)

Fig. 22: Optical images of bottom layer, reinforced with SiC particles: (a): 240 mesh, 20 wt% SiC reinforcement; (b): 1200 mesh, 20 wt% SiC reinforcement

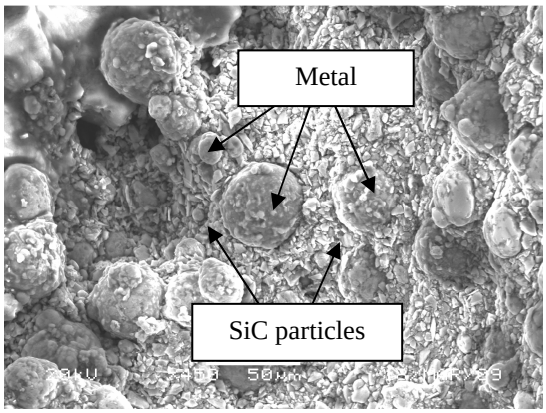

Fig. 23: SEM images of the crack in the bottom layer (from Exp. No. 4, with 1200 mesh SiC, 50 wt%)

The interfaces of the two layers have been investigated. As shown in Fig. 24, the part reinforced by large SiC particles also showed nice microstructures, indicating the two layers

were well bonded in the boundary. However, when the SiC particles are small (see Fig. 25), the two layers did not connected well because of the isolation of the metal powders.

.

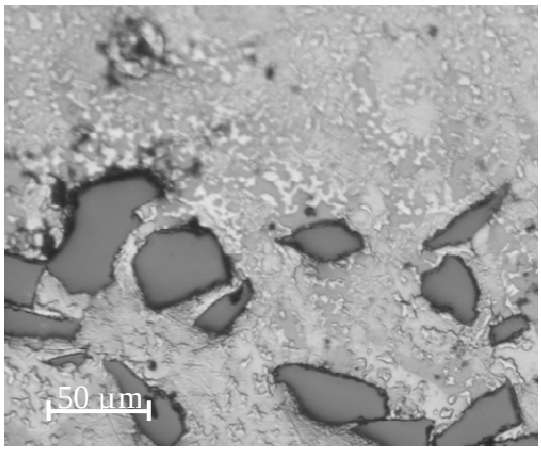

Fig. 24: Optical image of boundary layer (from Exp. No.1, with 20 wt% 240 mesh SiC)

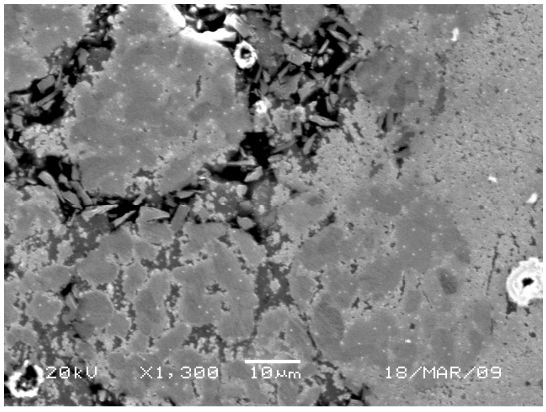

Fig. 25: SEM image of the boundary layer (from Exp. No. 2, with 20 wt% 1200 mesh SiC, note the top layer was shown in the right and bottom layer in the left)

The bonding interface between SiC and the metal phase is shown in Fig. 26. As shown in the figure, the roughness of the SiC particles affected the bonding significantly. When the interface is flat, the SiC particle and metal phase can bond tightly. However, for

the rough faces, the metal phase material was not able to fill in the course geometries, which produced clearance between the SiC particle and metal material.

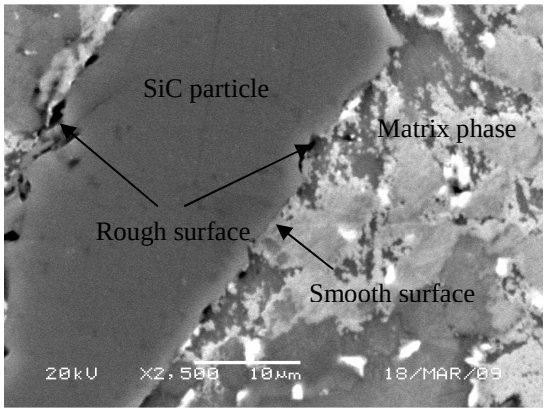

Fig. 26: SEM image of the bonding interface between SiC particle and metal phase

3.4.2 Hardness Test

The hardness of the parts was measured as shown in Fig. 27. Point 1 to point 5 show the hardness in the top layer, where 6 to 10 show the hardness in the SiC reinforced layers. It is observed that, the hardness fluctuated around 120 HV and did not change much in the top layer.

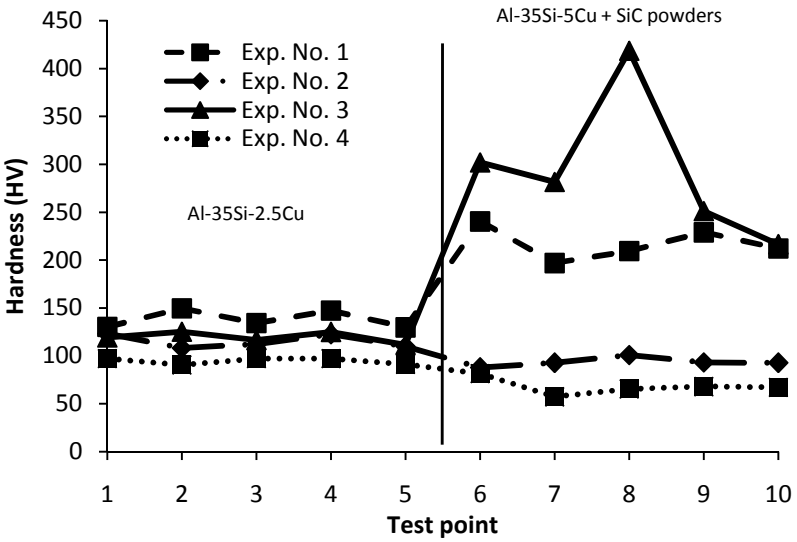

Fig. 27: Hardness test results

In the bottom layer, where the materials were reinforced by the SiC particles, the hardnesses of the parts were significantly different. The hardness of the layers reinforced with small size SiC was much lower than that of the large size. They are lower than the material without reinforcement. The reason for this is the loose, un-densified bottom microstructure formed in the part reinforced by small SiC particles. Note that the variance of hardness of SiC particles of Exp. No. 3 resulted from the local un-uniform distribution of SiC particles in the part. If the indent was made on or near the SiC particles, the hardness would be much higher than the other areas.

When the particles sizes are large, the hardness was significantly higher. It is observed that, the hardness increased from a mean value of 138.3 HV to 217.6 HV when reinforced by 20 wt% of SiC, and from 119.5 HV to 293.9 HV when reinforced by 50 wt% of SiC.

3.5 Conclusion

Functionally graded structures were successfully fabricated with semisolid powder processing. The effects of the reinforcement particle size and amount on the microstructure as well as the mechanical properties were investigated. The following conclusions can be drawn:

- The microstructure of the FGS was affected by the relative size of the reinforcement particles compared to the matrix powders. Denser parts can be obtained when reinforcement particles are larger than the base metal powders.
- The surface roughness of the reinforcement particles was important to the interface bonding between the SiC and matrix phase. Rough SiC face can result in small clearance between SiC and metal phases.
- The hardness increased significant when the material was reinforced with large size SiC particles. When small SiC was used, bonding did not occur due to isolation caused by the reinforcement phase.

3.6 Future Work

This chapter showed the preliminary result of application of semisolid powder processing in functionally graded structure. Further investigation will be conducted to study the effects of the size, amount and shape of the reinforcement particles on the microstructure, mechanical property and thermal property of the FGS. Investigation on the effect of the mechanical alloyed particles on forming process will also be performed.

CHAPTER 4. SUMMARY

4.1 Experimental Study of Viscosity and Phase Segregation of Al-Si Powders in the Semisolid State

In this study, the effects of the main processing parameters on the phase segregation and viscosity in the micro-scale semisolid powder processing were investigated by the design of experiment approach. Back extrusion experiments were performed and a mathematical method for quantifying the phase segregation was developed. The semisolid powder flow during the forming process was also studied. Based on the result of the parametric study, the following conclusion can be drawn.

1. Viscosity is significantly affected by the shear rate, extrusion ratio and the heating time. The viscosity increases as the shear rate, extrusion ratio and heating time decrease.
2. Phase segregation amount decreases as the shear rate increases and the extrusion ratio decreases. Heating time and pre-compaction pressure do not affect the phase segregation in the range studied in the experiments.
3. The semisolid powder flow in the back extrusion processing can be divided into three stages. It can be concluded that phase segregation occurs in the first stage. The second stage is a transient stage, in which the mixture of liquid and inter-connected solid phase is squeezed into the small gap. In the third stage, the force increased rapidly as the liquid phase is depleted underneath the punch.

4.2 Fabrication of Functionally Graded Structures by Semisolid Powder Processing

In this study, a two-layer FGS with one layer reinforced by SiC particles were fabricated with semisolid powder processing. The results indicate that SPP is capable of fabricating graded structures with promising microstructures and mechanical properties. In addition, the following conclusion can be drawn:

1. When the SiC particles are larger than the matrix powder, dense and strong parts can be formed. Smaller SiC particles can isolate the metal powders and resulting in porous and weak structures.
2. Smooth SiC particle surface can reinforce the interface bonding between SiC particles with matrix phase.
3. The hardness increased significant when the material was reinforced with large size SiC particles. When small SiC was used, bonding did not occur due to isolation caused by the reinforcement phase, resulting in a much lower hardness.

BIBLIOGRAPHY

1. Vollertsen, F., Schulze Niehoff, H., and Hu, Z., (2006), "State of the Art in Micro Forming," *International Journal of Machine Tools and Manufacture*, 46(11), 1172-1179.

2. Kim, G.-Y., Koc, M., Mayor, R., et al., (2007), "Modeling of the Semi-Solid Material Behavior and Analysis of Micro-/Mesoscale Feature Forming," *Journal of Manufacturing Science and Engineering, Transactions of the ASME*, 129(2), 237-245.

3. Kim, G.-Y., Ni, J., Mayor, R., et al., (2007), "An Experimental Investigation on Semi-Solid Forming of Micro/Meso-Scale Features," *Journal of Manufacturing Science and Engineering, Transactions of the ASME*, 129(2), 246-251.

4. Steinhoff, K., Weidig, U., and Weikert, J., (2004), "Micro Semi-Solid Manufacturing - a New Technological Approach Towards Miniaturisation," *Steel Research International*, 75(8-9), 611-619.

5. Backman, D. G., (1977), "Die Thermal Behavior in Machine Casting of Partially Solid High Temperature Alloys," *Metallurgical transactions. B, Process metallurgy*, 8(3), 471-477.

6. Spencer, D., Mehrabian, R., and Flemings, M., (1972), "Rheological Behavior of Sn-15 Pct Pb in the Crystallization Range," *Metallurgical and Materials Transactions B*, 3(7), 1925-1932.

7. Kumar, P., Martin, C., and Brown, S., (1993), "Shear Rate Thickening Flow Behavior of Semisolid Slurries," *Metallurgical and Materials Transactions A*, 24(5), 1107-1116.

8. Kang, S. G., Na, Y. S., Park, K. Y., et al., (2007), "A Study on the Micro-Formability of Al 5083 Superplastic Alloy Using Micro-Forging Method," *Materials Science and Engineering: A*, 449-451, 338-342.

9. Rath, S., (2006), "Investments for Casting Micro Parts with Base Alloys," *Microsystem technologies*, 12(3), 258.

10. Young, R. M. K., and Clyne, T. W., (1986), "A Powder-Based Approach to Semisolid Processing of Metals for Fabrication of Die-Castings and Composites," *Journal of Materials Science*, 21(3), 1057-1069.

11. Young, R. M. K., and Clyne, T. W., (1986), "A Powder Mixing and Preheating Route to Slurry Production for Semisolid Diecasting," *Powder metallurgy*, 29(3), 195-199.

12. Chen, C. M., Yang, C. C., and Chao, C. G., (2005), "A Novel Method for Net-Shape Forming of Hypereutectic Al-Si Alloys by Thixocasting with Powder Preforms," *Journal of Materials Processing Technology*, 167(1), 103-109.

13. Zu, L., and Luo, S., (2001), "Study on the Powder Mixing and Semi-Solid Extrusion Forming Process of Sicp/2024al Composites," *Journal of Materials Processing Technology*, 114(3), 189-193.

14. Hamilton, R. W., Zhu, Z., Dashwood, R. J., et al., (2003), "Direct Semi-Solid Forming of a Powder Sic-A1 Pmmc: Flow Analysis," *Composites Part A: Applied Science and Manufacturing*, 34(4), 333-339.

15. Luo, S.-J., Cheng, Y.-S., and Wang, P.-X., (2006), "Pseudo-Semi-Solid Thixoforging of Cup Shell with Al/Al2o3," *Transactions of Nonferrous Metals Society of China (English Edition)*, 16(4), 772-775.

16. Luo, S., Cheng, Y., and Du, Z., (2005), "Ceramics Matrix Composites Thixoforming in Pseudo-Semi-Solid State and the Preliminary Experimental Study," *Cailiao Yanjiu Xuebao/Chinese Journal of Materials Research*, 19(1), 107-112.

17. Chen, C. M., Yang, C. C., and Chao, C. G., (2004), "Thixocasting of Hypereutectic Al-25si-2.5cu-1mg-0.5mn Alloys Using Densified Powder Compacts," *Materials Science and Engineering A*, 366(1), 183-194.

18. El Wakil, S. D., (1992), "Extrusion of P/M Composites in the Semi-Solid State," *International Journal of Powder Metallurgy (Princeton, New Jersey)*, 28(2), 175-182.

19. Chen, C. M., Yang, C. C., and Chao, C. G., (2005), "Dry Sliding Wear Behaviors of Al-25si-2.5cu-1mg Alloys Prepared by Powder Thixocasting," *Materials Science and Engineering A*, 397(1-2), 178-189.

20. Quaak, C. J., and Kool, W. H., (1994), "Properties of Semisolid Aluminium Matrix Composites," *Materials Science and Engineering: A*, 188(1-2), 277-282.

21. Mclelland, A. R. A., Henderson, N. G., Atkinson, H. V., et al., (1997), "Anomalous Rheological Behaviour of Semi-Solid Alloy Slurries at Low Shear Rates," *Materials Science and Engineering A*, 232(1-2), 110-118.

22. Kopp, R., Neudenberger, D., and Winning, G., (2001), "Different Concepts of Thixoforging and Experiments for Rheological Data," *Journal of Materials Processing Technology*, 111(1-3), 48-52.

23. Kang, C. G., Jung, K. D., and Jung, H. K., (1999), "Control of Liquid Segregation of Semi-Solid Aluminum Alloys During Intelligent Compression Test," 1, 593-599.

24. Kim, W. Y., Kang, C. G., and Kim, B. M., (2007), "The Effect of the Solid Fraction on Rheological Behavior of Wrought Aluminum Alloys in Incremental Compression Experiments with a Closed Die," *Materials Science and Engineering: A*, 447(1-2), 1-10.

25. Suery, M., (1982), "Effect of Strain Rate on Deformation Behavior of Semi-Soliddendritic Alloys," *Metallurgical transactions. A, Physical metallurgy and materials science*, 13(10), 1809-1819.

26. Loue, W. R., Suery, M., and Querbes, J. L., (1993), "Microstructure and Rheology of Partially Remelted Alsi-Alloys," Cambridge, MA, USA, 266-275.

27. Gebelin, J. C., Suery, M., and Favier, D., (1999), "Characterisation of the Rheological Behaviour in the Semi-Solid State of Grain-Refined Az91 Magnesium Alloys," *Materials Science and Engineering A*, 272(1), 134-144.

28. Basner, T., Pehlke, R., and Sachdev, A., (2000), "Thin-Wall Back Extrusion of Partially Remelted Semi-Solid Sn-Pb," *Metallurgical and Materials Transactions A: Physical Metallurgy and Materials Science*, 31(1), 57-62.

29. Fan, Z., (2002), "Semisolid Metal Processing," *International Materials Reviews*, 47(49-85.

30. Kattamis, T. Z., (1991), "Rheology of Semisolid Al-4.5%Cu-1.5%Mg Alloy," *Materials science & engineering. A, Structural materials*, 131(2), 265-272.

31. Lashkari, O., and Ghomashchi, R., (2007), "The Implication of Rheology in Semi-Solid Metal Processes: An Overview," *Journal of Materials Processing Technology*, 182(1-3), 229-240.

32. Flemings, M. C., (1991), "Behavior of Metal Alloys in the Semisolid State," *Metallurgical transactions. A, Physical metallurgy and materials science*, 22(5),

33. Joly, P. A., and Mehrabian, R., (1976), "The Rheology of a Partially Solid Alloy," *Journal of Materials Science*, 11(8), 1393-1418.

34. Kiuchi, M., and Kopp, R., (2002), "Mushy/Semi-Solid Metal Forming Technology - Present and Future," *CIRP Annals - Manufacturing Technology*, 51(2), 653-670.

35. Laxmanan, V., (1980), "Deformation of Semi-Solid Sn-15 Pct Pb Alloy," *Metallurgical transactions. A, Physical metallurgy and materials science*, 11(12), 1927-1937.

36. Vieira, E. A., and Ferrante, M., (2005), "Prediction of Rheological Behaviour and Segregation Susceptibility of Semi-Solid Aluminium-Silicon Alloys by a Simple Back Extrusion Test," *Acta Materialia*, 53(20), 5379-5386.

37. Nicolli, L. C., Martin, C. L., Mo, A., et al., (2006), "Macrosegregation Caused by Deformation of the Mushy Zone," Miskolc-Lillafuered, Hungary, 508, 187-192.

38. Nicolli, L. C., Mo, A., and M'hamdi, M., (2005), "Modeling of Macrosegregation Caused by Volumetric Deformation in a Coherent Mushy Zone," *Metallurgical and Materials Transactions A: Physical Metallurgy and Materials Science*, 36 A(2), 433-442.

39. De Freitas, E. R., (2004), "Microstructure and Rheology of an Aa2024 Aluminium Alloy in the Semi-Solid State, and Mechanical Properties of a Back-Extruded Part," *Journal of Materials Processing Technology*, 146(2), 241-249.

40. Finke, S., (2002), "Solid Freeform Fabrication by Extrusion and Deposition of Semi-Solid Alloys," *Journal of Materials Science*, 37(15), 3101-3106.

41. Mola, J., Aashuri, H., and Shalchi, B., (2006), "Phase Segregation Susceptibility of Za27 Alloy at Different Shear Rates," Busan, South Korea, 116-117, 225-230.

42. Mola, J., Aashuri, H., and Amirkhiz, B. S., (2007), "Characterisation of Phase Segregation During Back Extrusion of Za27 Semisolid Alloy," *Materials Science and Technology*, 23(1), 113-118.

43. Kang, C. G., (1997), "A Finite-Element Analysis on the Upsetting Process of Semi-Solid Aluminum Material," *Journal of Materials Processing Technology*, 66(1-3), 76.

44. Ko, D. C., (2000), "Finite Element Analysis for the Semi-Solid State Forming of Aluminium Alloy Considering Induction Heating," *Journal of Materials Processing Technology*, 100(1-3), 95.

45. Saha, D., Apelian, D., and Dasgupta, R., (2004), "Ssm Processing of Hypereutectic Al-Si Alloys - an Overview," Limassol, Cyprus, 855-864.

46. Sanchez-Herencia, A. J., (2000), "Electrical Transport Properties in Zirconia/Alumina Functionally Graded Materials," *Journal of the European Ceramic Society*, 20(10), 1611-1620.

47. Bever, M. B., and Duwez, P. E., (1972), "Gradients in Composite-Materials," *Materials Science and Engineering*, 10(1), 1.

48. Birman, V., (2007), "Modeling and Analysis of Functionally Graded Materials and Structures," *Applied mechanics reviews*, 60(1), 195-216.

49. Movchan, B. A., (2002), "Functionally Graded Eb Pvd Coatings," *Surface & coatings technology*, 149(2), 252-262.

50. Basu, S. N., (2008), "Functionally Graded Chemical Vapor Deposited Mullite Environmental Barrier Coatings for Si-Based Ceramics," *Journal of the European Ceramic Society*, 28(2), 437-445.

51. Vaidya, R. U., (2002), "Use of Plasma Spraying in the Manufacture of Continuously Graded and Layered/Graded Molybdenum Disilicide/Alumina Composites," *Journal of thermal spray technology*, 11(3), 409-414.

52. Smurov, I., (2008), "Laser Cladding and Laser Assisted Direct Manufacturing," *Surface & coatings technology*, 202(18), 4496-4502.

53. Sidky, P. S., (1999), "Review of Inorganic Coatings and Coating Processes for Reducing Wear and Corrosion," *British Corrosion Journal*, 34(3), 171-183.

54. Ruigang, W., (2002), "Investigation of the Physical and Mechanical Properties of Hot-Pressed Machinable Si_3N_4/H-BN Composites and FGM," *Materials science & engineering. B, Solid-state materials for advanced technology*, 90(3), 261-268.

55. Kawasaki, A., (1997), "Concept and P/M Fabrication of Functionally Gradient Materials," *Ceramics international*, 23(1), 73-83.

56. Chu, J., (1993), "Slip Casting of Continuous Functionally Gradient Material," *Journal of the Ceramic Society of Japan*, 101(7), 818-820.

57. Rodriguez-Castro, R., (2002), "Processing and Microstructural Characterization of Functionally Gradient Al A359/SiC_P Composite," *Journal of Materials Science*, 37(9), 1813-1821.

58. Watanabe, Y., (1998), "Control of Composition Gradient in a Metal-Ceramic Functionally Graded Material Manufactured by the Centrifugal Method," *Composites. Part A, Applied science and manufacturing*, 29(5), 595-601.

59. Gupta, M., (2002), "Synthesis and Characterization of a Free-Standing, One-Dimensional, Al-Cu/SiC-Based Functionally Graded Material," *Journal of Materials Synthesis and Processing*, 10(2), 75-81.

60. Corbin, S. F., (1999), "Functionally Graded Metal/Ceramic Composites by Tape Casting, Lamination and Infiltration," *Materials science & engineering. A, Structural materials*, 262(1), 192-203.

61. Pech-Canul, M. I., (2002), "Effect of Processing Parameters on the Production of Bilayer-Graded Al/SiC_P Composites by Pressureless Infiltration," *Materials letters*, 56(4), 460-464.

62. Song, D. H., Park, Y. H., Park, Y. H., et al., (2007), "Thermomechanical Properties of Functionally Graded Al-SiCp Composites," *Materials Science Forum*, 534-536(1565-1568.

63. Pech-Canul, M. I., Parras-Medecigo, E. E., and Rodriguez-Reyes, M., (2002), "Effect of processing parameters on the formation of composite-composite interfaces in bilayer Al/SiCp composites," 203-208.

64. Velhinho, A., Sequeira, P. D., Braz Fernandes, F., et al., (2003), "Al/SiCp Functionally Graded Metal-Matrix Composites Produced, by Centrifugal Casting: Effect of Particle Grain Size on Reinforcement Distribution," *Materials Science Forum*, v 423-425, 257-262.

65. Rodriguez-Castro, R., (2002), "Microstructure and Mechanical Behavior of Functionally Graded Al A359/SiC_P Composite," *Materials science & engineering. A, Structural materials*, 323(1), 445-456.

66. Watari, F., (1997), "Fabrication and Properties of Functionally Graded Dental Implant," *Composites. Part B, Engineering*, 28(1), 5-11.

67. Lin, C. Y., (1999), "Production of Silicon Carbide Al 2124 Alloy Functionally Graded Materials by Mechanical Powder Metallurgy Technique," *Powder metallurgy*, 42(1), 29-33.

68. Cho, K.-M., Choi, I.-D., and Park, I., (2004), "Thermal Properties and Fracture Behavior of Compositionally Graded Al-Sicp Composites," *Materials Science Forum*, 449-452(1), 621-624.

69. Corbin, S. F., (2003), "Cladding of an Fe-Aluminide Coating on Mild Steel Using Pulsed Laser Assisted Powder Deposition," *Materials science & engineering. A, Structural materials*, 354(1), 48-57.

70. Krantz, T., (2004), "Increased Surface Fatigue Lives of Spur Gears by Application of a Coating," *Journal of mechanical design*, 126(6), 1047-1054.

71. Ramalingam, S., (1984), "1984," Gaitherburg, MD, USA, 3-17.

72. Yasue, K., (2000), "Elemental Blended Powders Semisolid Forming of Ti-Al Based Alloys," *Journal of Materials Science*, 35(23), 5927-5932.

73. Wen, C. E., (2001), "Fabrication of Tial by Blended Elemental Powder Semisolid Forming," *Journal of Materials Science*, 36(7), 1741-1745.

74. Ward, P. J., Atkinson, H. V., Anderson, P. R. G., et al., (1996), "Semi-Solid Processing of Novel Mmcs Based on Hypereutectic Aluminium-Silicon Alloys," *Acta Materialia*, 44(5), 1717-1727.